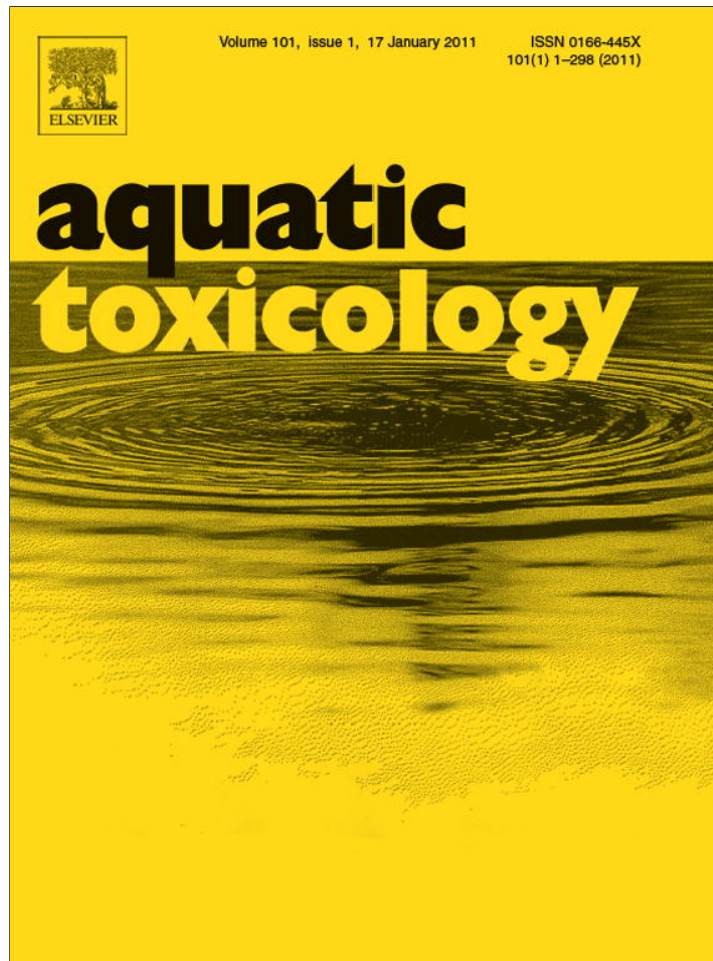


Provided for non-commercial research and education use.  
Not for reproduction, distribution or commercial use.



(This is a sample cover image for this issue. The actual cover is not yet available at this time.)

This article appeared in a journal published by Elsevier. The attached copy is furnished to the author for internal non-commercial research and education use, including for instruction at the authors institution and sharing with colleagues.

Other uses, including reproduction and distribution, or selling or licensing copies, or posting to personal, institutional or third party websites are prohibited.

In most cases authors are permitted to post their version of the article (e.g. in Word or Tex form) to their personal website or institutional repository. Authors requiring further information regarding Elsevier's archiving and manuscript policies are encouraged to visit:

<http://www.elsevier.com/copyright>



Contents lists available at SciVerse ScienceDirect

# Aquatic Toxicology

journal homepage: [www.elsevier.com/locate/aquatox](http://www.elsevier.com/locate/aquatox)

## Mercury effects on *Thalassiosira weissflogii*: Applications of two-photon excitation chlorophyll fluorescence lifetime imaging and flow cytometry

Yun Wu<sup>a</sup>, Yan Zeng<sup>b</sup>, Jianan Y. Qu<sup>b</sup>, Wen-Xiong Wang<sup>a,\*</sup><sup>a</sup> Division of Life Science, Hong Kong University of Science and Technology (HKUST), Clear Water Bay, Kowloon, Hong Kong, PR China<sup>b</sup> Department of Electronic and Computer Engineering, Hong Kong University of Science and Technology (HKUST), Clear Water Bay, Kowloon, Hong Kong, PR China

### ARTICLE INFO

#### Article history:

Received 26 October 2011

Received in revised form

20 December 2011

Accepted 3 January 2012

#### Keywords:

Phytoplankton

Inorganic mercury

Methylmercury

Fluorescence lifetime

Population development

### ABSTRACT

The toxic effects of inorganic mercury [Hg(II)] and methylmercury (MeHg) on the photosynthesis and population growth in a marine diatom *Thalassiosira weissflogii* were investigated using two methods: two-photon excitation fluorescence lifetime imaging (FLIM) and flow cytometry (FCM). For photosynthesis, Hg(II) exposure increased the average chlorophyll fluorescence lifetime, whereas such increment was not found under MeHg stress. This may be caused by the inhibitory effect of Hg(II) instead of MeHg on the electron transport chain. For population growth, modeled specific growth rate data showed that the reduction in population growth by Hg(II) mainly resulted from an increased number of injured cells, while the live cells divided at the normal rates. However, MeHg inhibitory effects on population growth were contributed by the reduced division rates of all cells. Furthermore, the cell images and the FCM data reflected the morphological changes of diatom cells under Hg(II)/MeHg exposure vividly and quantitatively. Our results demonstrated that the toxigenicity mechanisms between Hg(II) and MeHg were different in the algal cells.

© 2012 Elsevier B.V. All rights reserved.

### 1. Introduction

Mercury pollution has raised great concern since 1950s with the outbreak of Minamata disease in Japan, which was caused by the consumption of highly mercury-contaminated fish. Since then, many studies have been conducted on the toxic effects of mercury on animals (including humans) (Eisler, 1987; Clarkson, 1997). The possible mechanisms of mercury toxicity include its binding with the thiol group of functional enzymes, replacing the essential ions and producing oxidative stress. Despite the fact that the contamination by mercury in aquatic ecosystem has been widely reported, toxic effects of mercury on phytoplankton, the primary producers at the base of aquatic food webs, have not drawn much attention.

Mercury exerts its toxicity on one of the most important metabolic processes in phytoplankton, namely photosynthesis. Mercury compounds strongly inhibit photosynthetic electron transport with many action sites: the donor side of PSI (Miles et al., 1973; Singh et al., 1989), the acceptor side of PSI (Mi et al., 2000), the core of PSI (Šeršeň et al., 1998), the donor side of PSII (Bernier et al., 1993), the acceptor side of PSII (Prokowski, 1993), the core of PSII (Murthy et al., 1995), and the light harvesting complex II (Nahar and Tajmir-Riahi, 1995). To evaluate the

toxicity of contaminants to photosystem, pulse-amplitude-modulation (PAM) fluorescence method was developed to detect parameters that reflect the photosynthetic electron-transport activity *in vivo*. However, parameters such as maximum photosynthetic system II quantum yield and operational photosynthetic system II quantum yield were less sensitive than the specific growth rate in some cases (Miao et al., 2005; Wang and Wang, 2008). Recently, a sensitive, rapid imaging method – two-photon excited fluorescence lifetime imaging (TPE-FLIM) was built to provide microscopic fluorescence imaging and fluorescence lifetime information, reflecting the intrinsic energy status of fluorescent molecules. Chlorophyll *a* fluorescence imaging can be done using two-photon excitation – the fluorescent molecules are excited by simultaneously absorbing two near-infrared photons (Tirlapur and König, 2001). Moreover, any inhibition on the electron transport chain, which blocks the photochemical quenching, will lead to the increment of the fluorescence lifetime (Broess et al., 2009). Previous study has demonstrated that under the stress of an inhibitor 3-(3,4-dichlorophenyl)-1,1-dimethyl urea (DCMU; blocking the electron transport chain), significant increase could be observed in the average chlorophyll fluorescence lifetime (Petrášek et al., 2005). Similar phenomenon was also shown in algae treated with DCMU (Zeng et al., unpublished). Therefore, TPE-FLIM could be adopted to investigate the photosynthetic toxicity caused by mercury.

Growth inhibition is another widely used endpoint to assess metal toxicity. Standard toxicity tests using microalgae translate the contaminant effects to the concentration at which the specific

\* Corresponding author.

E-mail address: [wwang@ust.hk](mailto:wwang@ust.hk) (W.-X. Wang).

growth rate of the population is reduced by 50% compared to the control ones. Although simple and easy to conduct, such method requires that the responses of all cells are completely in line and uses the average behavior of population to stand for the individual behavior. Under stress conditions, the reduction in growth rate at population levels may result from two reasons: decreased cell division rate and increased injured/dead cell numbers. However, traditional microscopic methods cannot distinguish between these two. The application of flow cytometry (FCM) in aquatic microbiology can analyze phytoplankton behavior at both the population and single cell levels. Together with various specific-binding fluorescence dyes, FCM can be used to evaluate the cellular physiological states (Wang et al., 2010) and to provide more information about pollutant toxicity mechanisms.

Taking all these factors into consideration, the aim of this study was to investigate the toxic effects of Hg(II) and MeHg on a model marine phytoplankton *Thalassiosira weissflogii*. The images of cells and average chlorophyll fluorescence lifetime distribution were quantified by two photon excitation fluorescence lifetime imaging method. Flow cytometry approaches were also used to assess the mercury effects on cell morphology (including cell size, cell complexity), photosynthesis (autofluorescence), and growth kinetics (cell counting and cell viability). We calculated the specific growth rate for all cells and for live cells only, and then compared the different effects between Hg(II) and MeHg on both photosynthesis and growth inhibition.

## 2. Materials and methods

### 2.1. Diatom cultures and experimental design

The marine diatom, *T. weissflogii* (CCMP 1587, taxonomic authority: (Grun.) Fryxell et Hasle, Class Coscinodiscophyceae), obtained from the Provasoli-Guillard National Center for Culture of Marine Phytoplankton, was grown in sterile f/2 medium. The strain was maintained at  $22 \pm 1$  °C under  $80 \mu\text{mol photons m}^{-2} \text{s}^{-1}$  with a light: dark cycle of 14:10 h. The seawater used in this study was collected from 10 km off the Eastern Hong Kong shore and was filtered through a  $0.22 \mu\text{m}$  GP Express PLUS Membrane (Sericap Millipore Corporation). The algal cells were transferred from the f/2 medium to the f/2–f/20 (levels of trace metals were 10 times less) medium (without EDTA, Cu and Zn addition) for one week acclimation before the experiments.

Hg(II) (Sigma, St. Louis, MO), dissolved in 1 M ultrapure HCl (BDH, Poole, UK) and MeHg stock solution (Brooks Rand, USA) were added into the f/2–f/20 (-EDTA, Cu and Zn) medium. After addition of suprapure NaOH (1 M) to adjust the pH of the medium to  $8.2 \pm 0.1$ , the exposure medium was equilibrated overnight before use. There were six concentration levels and each with two replicates for both Hg(II) and MeHg. The nominal concentrations were 0.0, 0.2, 0.4, 0.7, 0.9 and  $1.1 \mu\text{M l}^{-1}$  for Hg(II); and 0.0, 4.6, 9.3, 18.6, 23.2 and  $27.8 \text{ nM l}^{-1}$  for MeHg, respectively. The initial cell density for all treatments was  $5 \times 10^4 \text{ cells ml}^{-1}$ . All the experiments were conducted under the same temperature, irradiance and light/dark regime conditions described above and lasted for 72 h.

### 2.2. Imaging and fluorescence lifetime analysis instrumentation

After acclimation, the diatom cells in the mid-exponential growth phase were harvested by centrifugation (3000 rpm, 24 °C, 5 min) and then immediately resuspended into the Hg(II) and MeHg exposure medium. At the end of exposure (72 h), cells were collected for fluorescence analysis. A custom-built two-photon excitation Fluorescence lifetime imaging (TPE-FLIM) microscope employed a femtosecond Ti-sapphire laser (Mira 900, Coherent)

tuned at 850 nm as the excitation source. The collimated excitation beam was focused onto the sample by a water immersion objective (40 $\times$ , 1.1 numerical aperture (NA), Zeiss). A pair of galvo mirrors was utilized to create a sampling area of  $75 \mu\text{m} \times 75 \mu\text{m}$ . The scanning depth was manipulated by an actuator (Model Z625B, Thorlabs). The algae were placed directly on the glass slides using a pipette and sandwiched by a cover glass. A dichroic mirror (760 nm, Chroma) was applied to separate the excited epifluorescence from the excitation pulses. A short pass filter (740 nm, Chroma) and a bandpass filter ( $675 \pm 25 \text{ nm}$ , Chroma) were used to further purify the fluorescence signal. The photo multiplier tube (PMT) with a time-correlated single photon counting (TCSPC) module (PML-100-20 and SPC-730, Becker & Hickl GmbH) was applied to measure the fluorescence signal. The integrated time was set at 8 s. Such sectioning images were collected from each replicate and the minimum separated distance among these images was larger than  $500 \mu\text{m}$ . All the measurements for each replicate were completed within 30 min after sample preparation. The fluorescence lifetime analysis for each image pixel was achieved by applying an incomplete dual exponential fitting model,  $A_1 \exp(-t/\tau_1) + A_2 \exp(-t/\tau_2) + A_1 \exp[-(t + \Delta\tau)/\tau_1] + A_2 \exp[-(t + \Delta\tau)/\tau_2]$ , after the decay curve was deconvoluted with system response by commercial software (SPCImage, Becker & Hickl GmbH).  $\tau_1$  and  $\tau_2$  are the lifetime components while  $A_1$  and  $A_2$  are the amplitudes of two decay terms, respectively. The lifetime detecting range of the TCSPC module for each excitation pulse  $\Delta\tau$  was 12.5 ns, determined by the pulse repetition rate (80 MHz). The average fluorescence lifetime was calculated using equation:  $\tau_{\text{average}} = A_1 \tau_1 + A_2 \tau_2$ . High signal-to-noise ratio image pixels were extracted by a developed image guided method (Iwai et al., 2010). The average fluorescence lifetime distribution for each treated group samples was obtained by statistically analyzing the extracted pixels from at least 5 images.

### 2.3. Flow cytometry measurements

Propidium iodide (PI; Sigma, St. Louis, MO, USA) was used to assess the cell viability due to its membrane permeability. Cells were stained with PI according to the protocol of the supplier (Molecular Probes, Invitrogen) and with some modifications from Franklin et al. (2001). The viability of cells was expressed as the percentage of live cell numbers with respect to the total cells numbers.

Flow cytometry (FCM) analysis was carried out at the following time points: 0, 14, 24, 38, 48, 62 and 72 h, according to the light/dark cycle. Two 1 ml aliquots were collected from each beaker: a 1 ml sample without staining by PI for cell number, size, complexity and autofluorescence determination, and another 1 ml aliquot stained by PI for membrane integrity test. Data were acquired with a FAC-SCalibur flow cytometer (BD Biosciences, Erembodegem, Belgium), equipped with a 15 mW laser (488 nm). Autofluorescence of chlorophyll *a* (FL3; >650 nm) was used as the gate to exclude non-algal particles. PI fluorescence was acquired in the FL2 (564–606 nm) channel. Since the forward light scatter (FSC) and side light scatter (SSC) were correlated with the cell size and cell complexity, respectively (Shapiro, 1995), light scatter signals were expressed as the geometric mean values (calibrated by the  $10 \mu\text{m}$  YG beads, Fluoresbrite, Polysciences, Warrington, PA) from density plot in arbitrary units (a.u.) to show the potential change of cell size and structure under mercury stress. In the same way, autofluorescence was analyzed to study the response of chlorophyll *a*. Quantification was based on the flow rate calibration method (Marie et al., 2005) and then the cell density was calculated as the number of cells acquired/(sample flow rate  $\times$  acquisition time). The total cell density was considered as the sum of both live and injured cells.

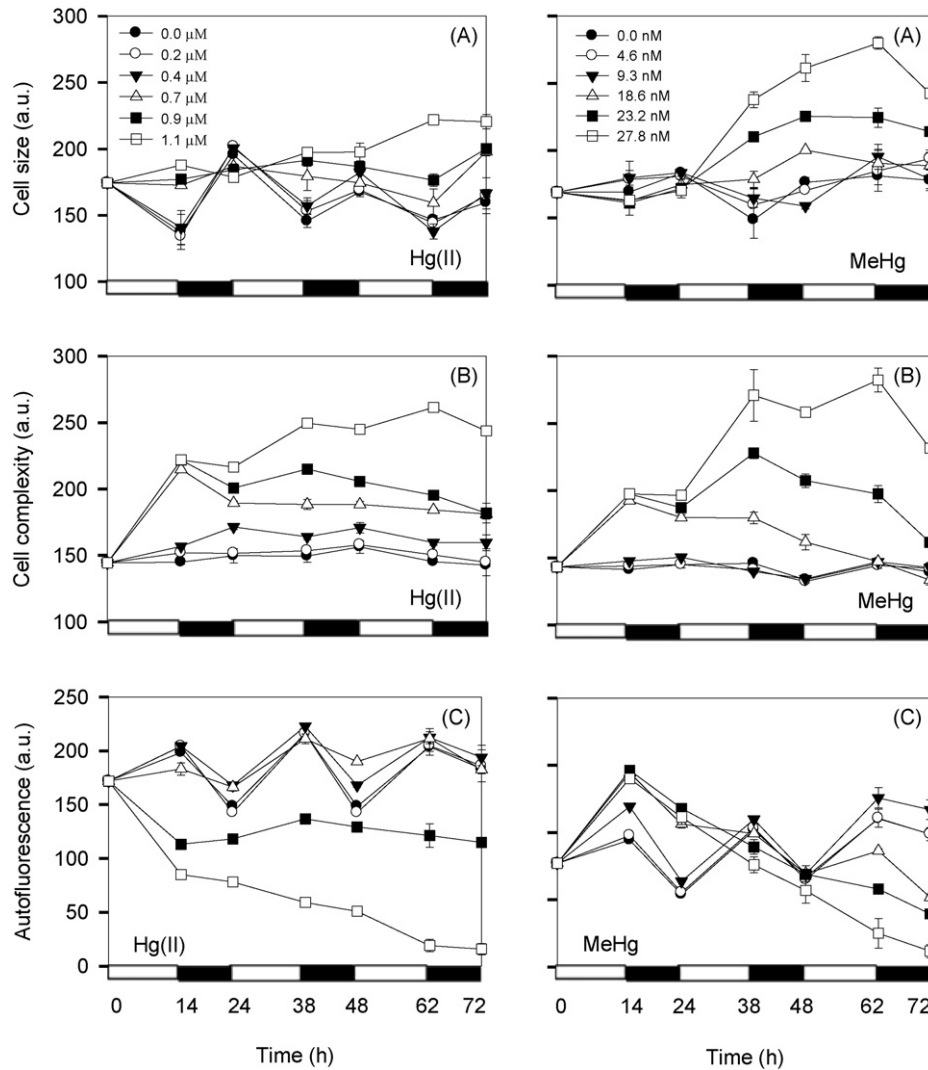


**Fig. 1.** Changes in cell size (A), complexity (B), and autofluorescence (C) of *T. weissflogii* with time under different Hg(II) and MeHg exposure concentrations. White and dark bars indicate light and dark periods, respectively. Data are mean  $\pm$  SD ( $n=2$ ).

FCM data were stored as listmode files and statistically analyzed by WinMDI software (version 2.9). Exponentially growing and 4% formaldehyde-killed *T. weissflogii* suspensions were used to distinguish live (with low PI fluorescence) and dead/injured (with high PI fluorescence) cells. Then the specific growth rate  $\mu$  ( $\text{h}^{-1}$ ) of the diatom cells was calculated according to the function presented by Czechowska and Van Der Meer (2011) as follows:

$$\mu = \frac{1}{\Delta t} \ln \frac{N_t - N_{t-\Delta t}(1 - V)}{N_{t-\Delta t}V}$$

where  $N_t$  is the total cell density at time  $t$ ,  $N_{t-\Delta t}$  is the total cell density at time  $t - \Delta t$ ,  $V$  is the cell viability at time  $t - \Delta t$ , and  $\Delta t$  is the time interval (h). The assumption of this model was that the injured cells could not divide but were still counted at time  $t$ . Two methods were used to assess the cell growth under mercury stress: (i) traditional toxicity test, in which  $V=1$  (assuming that all cells were alive at each time point), to predict the whole cells growth performance; (ii) data approach method, in which  $V$  was measured at each time point in the experiments. The average specific growth rate  $\mu$  was normalized to the value of the control treatment (=100%).

### 3. Results

#### 3.1. Cell morphology

The changes of the size and complexity of *T. weissflogii* cells under different levels of Hg(II) and MeHg stress are shown in Fig. 1A and B. At low Hg(II) or MeHg levels, *T. weissflogii* cells showed obvious light/dark cycle in cell size, i.e., a decrease in cell size throughout the periods of light and an increase during the dark conditions (except for those under MeHg treatment during 48–72 h). When the concentrations were above  $0.4 \mu\text{M}$  and  $9.3 \text{ nM}$  for Hg(II) and MeHg, respectively, such phenomenon disappeared and the so-called cell swelling happened. At the highest Hg(II) concentration, cell size showed a slight increase after 72 h exposure compared to the beginning ( $26.4 \pm 3.0\%$ ), and the most pronounced enlargement was observed at the highest MeHg concentrations after 62 h of exposure ( $65.7 \pm 1.4\%$ ). As for the cell complexity, its change had no relationship with light/dark cycle either for Hg(II) or MeHg exposure. However, it increased with exposure concentration for both Hg(II) and MeHg.

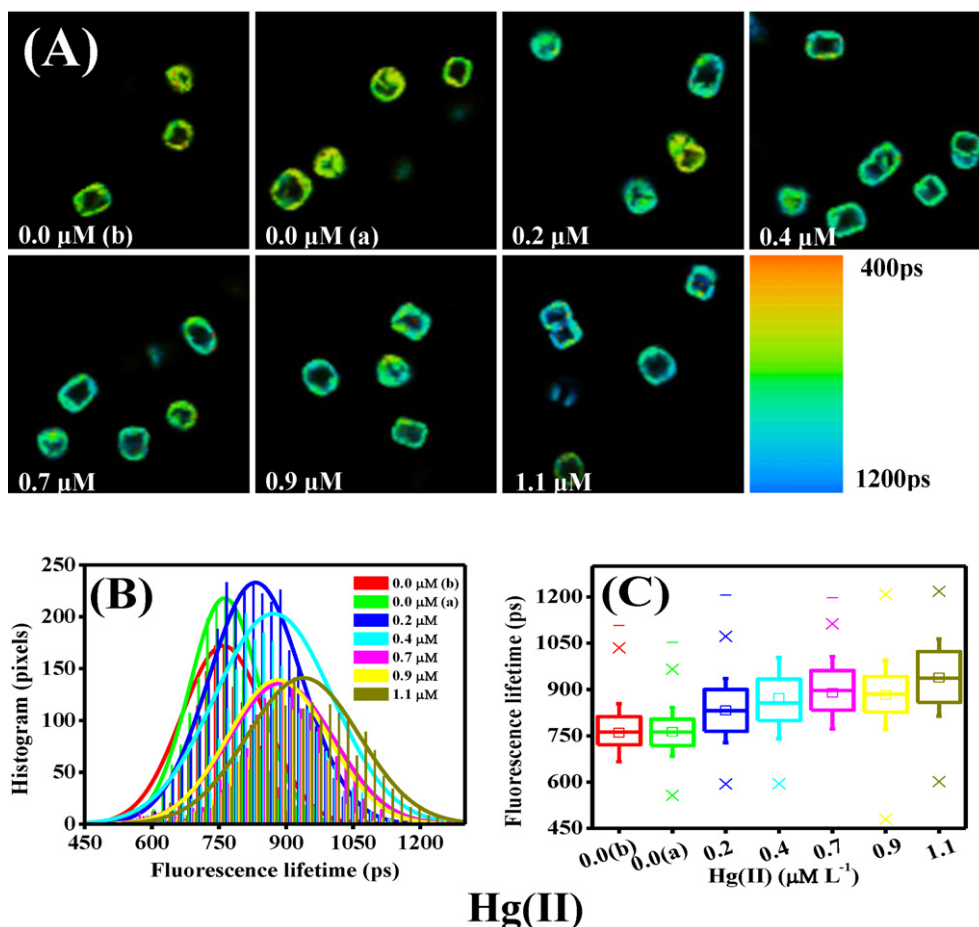


**Fig. 2.** Average fluorescence lifetime images of *T. weissflogii* exposed to different concentrations of Hg(II) (A); histogram analysis of fluorescence lifetime distributions (B); box analysis of fluorescence lifetime (C) (reticular: mean value; cross: 1–99% of the corresponding distribution; box size: 25–75% of the corresponding distribution; straight line: median) (b) 0.0 μM at 0 h, before exposure; (a) 0.0 μM at 72 h, after exposure). Data are mean ± SD (n=2).

### 3.2. Photosynthesis

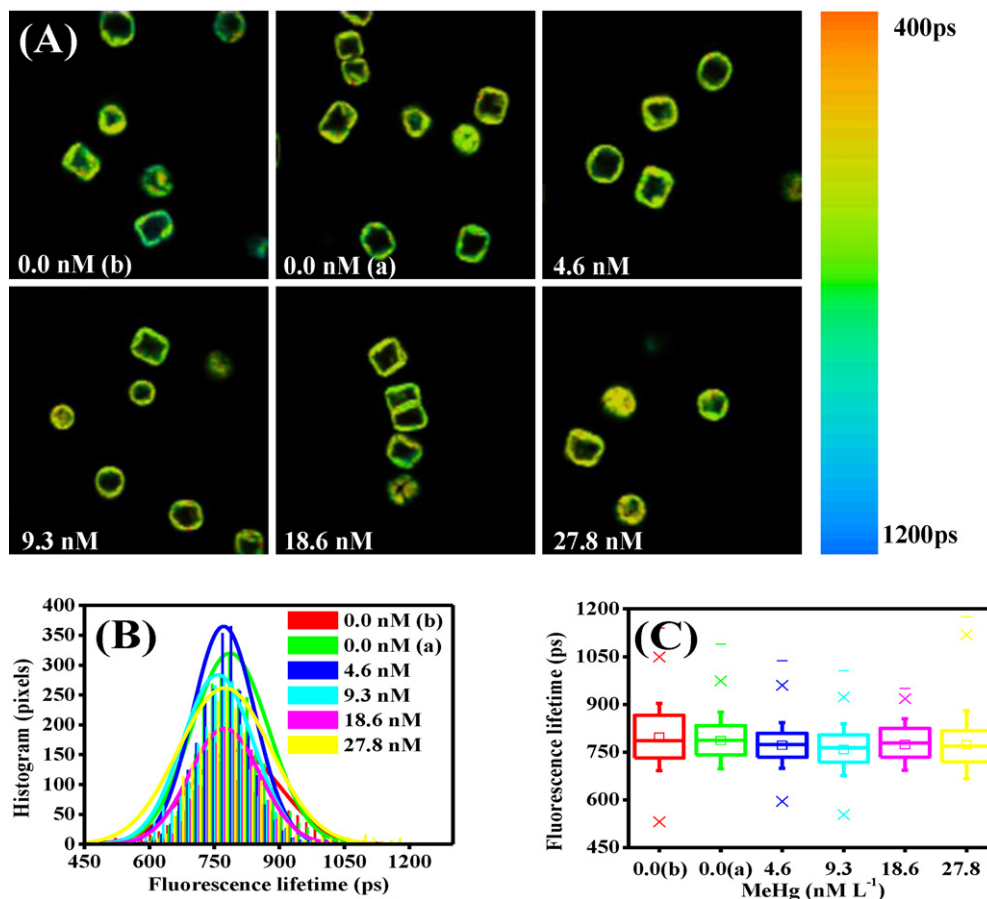
A marked light/dark cycle of autofluorescence signals after exposure to lower levels of Hg(II) and MeHg is shown in Fig. 1C. Different from the alteration in cell size, the autofluorescence of *T. weissflogii* cells kept increasing during the daytime and decreased in the darkness when the concentrations were below 0.9 μM and 23.2 nM for Hg(II) and MeHg, respectively. With increasing Hg(II)/MeHg stress, autofluorescence decreased with exposure time, with a few exceptions, indicating some damage or dysfunction of the chlorophyll *a* in the diatom cells.

The average chlorophyll fluorescence lifetime images (Figs. 2 and 3) could also give clues on the photosynthesis activity after exposure to mercury. With increasing Hg(II) concentrations, visible average fluorescence lifetime enhancement after 72 h exposure was recorded in the sectioning color-coded images, from yellow–green to green–blue. Fig. 2B shows the histogram analysis of fluorescence lifetime distributions and exhibits an obvious peak shift. The fluorescence lifetime peak distribution of control treatment was about 760 ps, moving up to ~940 ps after 72 h exposure to 1.1 μM of Hg(II). Statistical analysis (Fig. 2C) further proved an increasing trend of average chlorophyll fluorescence lifetime with increasing Hg(II) exposure. In contrast, such increases were not observed under MeHg exposure (Fig. 3), even at the highest MeHg concentration that could totally inhibit the cell growth.

### 3.3. Population development

The gates used to identify the cell viability and typical PI fluorescence histogram before and after mercury addition are given in Fig. 4. Table 1 presents the calculated cell viability of *T. weissflogii* assayed by FCM. The viability of diatom cells decreased significantly at higher mercury levels. However, their responses to Hg(II) and MeHg were quite different. The cell viability was less than 10% after 72 h exposure to 1.1 μM Hg(II), while it remained more than 80% for all MeHg concentrations during the experiments.

Under Hg(II)/MeHg stress, the normalized overall population specific growth rate is shown in Fig. 5. The control growth rates for Hg(II) and MeHg were  $0.028 \pm 0.000 \text{ h}^{-1}$  and  $0.026 \pm 0.000 \text{ h}^{-1}$ , respectively (with CV% < 10%). In the presence of toxic Hg, the overall population growth diminished significantly compared to the controls. In the case of Hg(II), a nominal concentration of 0.4 μM did not have inhibition effect on the population growth, whereas this value for MeHg was 9.3 nM. The highest metal concentration resulted in up to  $90.3 \pm 4.9\%$  and 100% growth inhibition for Hg(II) and MeHg, respectively. With the assumption that only live cells were able to reproduce, the live cells specific growth rate was modeled (Fig. 5). Interestingly, the situation was completely different between Hg(II) and MeHg. Upon exposure to Hg(II), the actual specific growth rate of the live cells did not decrease significantly or even increased, while for MeHg the specific growth rates of the live cells and total cells were comparable ( $p > 0.5$  at each concentration),



### MeHg

**Fig. 3.** Average fluorescence lifetime images of *T. weissflogii* exposed to different concentrations of MeHg (A); histogram analysis of fluorescence lifetime distributions (B); box analysis of fluorescence lifetime (C) (reticular: mean value; cross: 1–99% of the corresponding distribution; box size: 25–75% of the corresponding distribution; straight line: median) ((b) 0.0 nM at 0 h, before exposure; (a) 0.0 nM at 72 h, after exposure). Data are mean ± SD ( $n = 2$ ).

indicating differences in the underlying toxic mechanisms of these two Hg species.

#### 4. Discussion

Generally, the toxic concentration range for MeHg was 1–2 orders of magnitude lower than that of Hg(II) to phytoplankton

species. As expected, MeHg showed higher toxicity than Hg(II) on the growth of *T. weissflogii* in this study. Such differences between mercury species could be related to the cellular photosynthesis responses (pigment synthesis and photosynthesis electron transport), the growth inhibition patterns caused by mercury compounds, and greater uptake potential of MeHg into algal cells. It should be noted that the toxic concentrations used were 2–3 orders

**Table 1**  
Cell viability of diatoms *Thalassiosira weissflogii* at each time point under different levels of Hg(II) and MeHg exposure.

	Viability (%)					
	14 h	24 h	38 h	48 h	62 h	72 h
<b>Hg (II) (<math>\mu\text{M}</math>)</b>						
0.0	100.0 ± 0.0	99.8 ± 0.0	99.2 ± 0.0	99.6 ± 0.1	100.0 ± 0.0	100.0 ± 0.0
0.2	100.0 ± 0.0	99.8 ± 0.0	99.9 ± 0.1	100.0 ± 0.0	99.8 ± 0.0	99.7 ± 0.0
0.4	99.9 ± 0.0	99.7 ± 0.0	99.9 ± 0.0	99.8 ± 0.0	99.8 ± 0.0	99.6 ± 0.0
0.7	87.9 ± 3.6*	96.5 ± 4.5	97.2 ± 0.6*	96.3 ± 0.4**	97.0 ± 0.6*	97.8 ± 0.3*
0.9	37.0 ± 0.0***	41.4 ± 0.8***	62.9 ± 2.3**	71.0 ± 0.5***	78.0 ± 0.4***	82.5 ± 0.2***
1.1	2.8 ± 0.4***	15.3 ± 1.0***	19.3 ± 1.7***	17.9 ± 0.3***	4.9 ± 2.6***	5.7 ± 2.9***
<b>MeHg (nM)</b>						
0.0	100.0 ± 0.0	100.0 ± 0.0	99.2 ± 0.1	99.9 ± 0.0	100.0 ± 0.1	100 ± 0.0
4.6	99.8 ± 0.1	99.6 ± 0.0	99.7 ± 0.0	99.6 ± 0.1	99.2 ± 0.0	99.5 ± 0.0
9.3	97.7 ± 0.1***	100.0 ± 0.0	100.0 ± 0.0	99.5 ± 0.0	99.8 ± 0.0	99.9 ± 0.0
18.6	88.2 ± 2.5*	91.1 ± 0.3***	93.5 ± 0.1***	95.7 ± 0.1***	95.6 ± 0.3**	96.5 ± 0.7*
23.2	87.8 ± 0.2***	87.8 ± 0.2***	89.5 ± 0.7**	90.4 ± 0.3***	88.0 ± 0.6**	89.1 ± 0.7**
27.8	86.7 ± 1.7**	87.5 ± 0.9**	85.4 ± 1.9**	86.4 ± 2.0*	83.6 ± 2.7*	81.7 ± 1.7**

Asterisks indicate statistically significant differences compared with the controls (\* $p < 0.05$ , \*\* $p < 0.01$ , \*\*\* $p < 0.001$ ,  $t$ -test). Data are means ± SD ( $n = 2$ ).

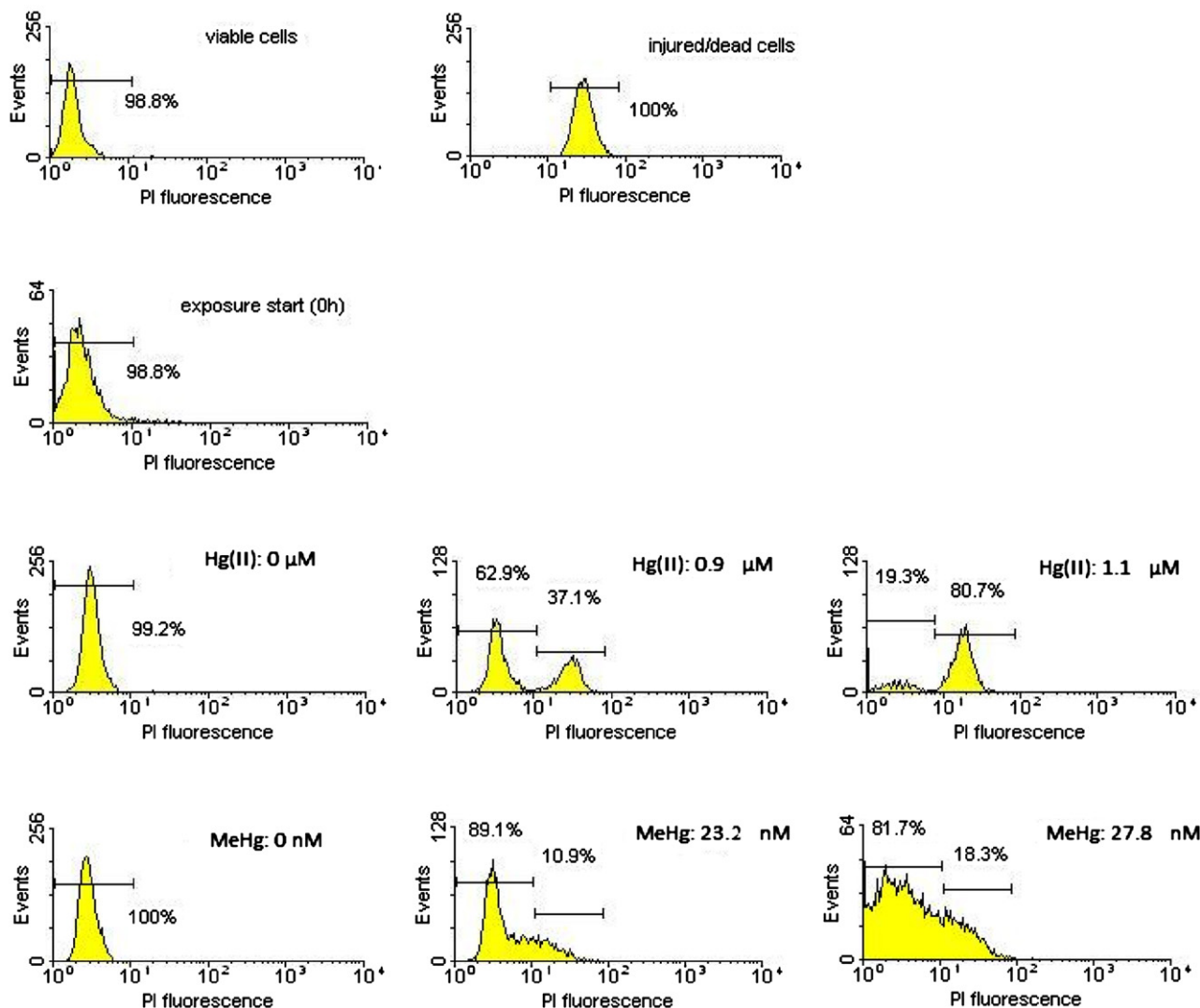


**Fig. 4.** Monoparametric histogram of flow cytometric analysis of the cell viability of *T. weissflogii*. (A) Exponentially growing and 4% formaldehyde killed diatom to determine the gates for live and injured/dead subpopulations, respectively; (B) under non-exposed conditions at time 0 h; (C) after 38 h of exposure to different Hg(II) concentrations; (D) after 72 h of exposure to different MeHg concentrations. Data are mean  $\pm$  SD ( $n=2$ ).

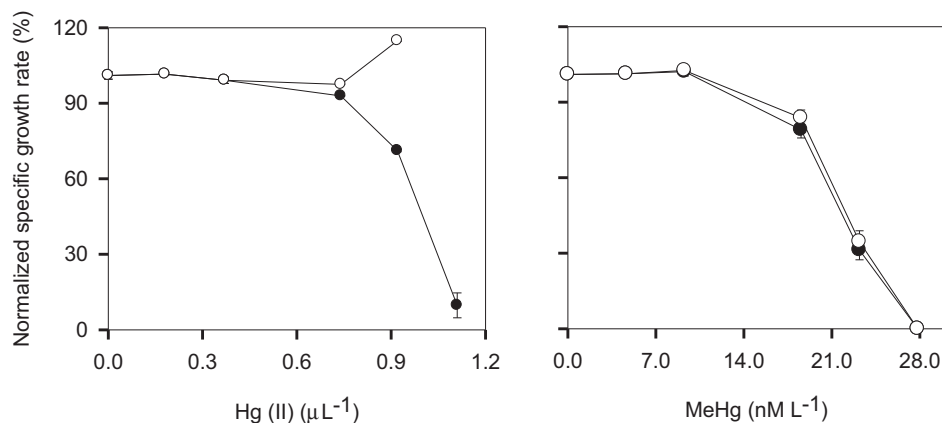


**Fig. 5.** Changes in the normalized specific growth rate  $\mu$  of *T. weissflogii* at different exposure concentrations of Hg(II) and MeHg. Closed symbols represent the calculated normalized growth rates with the assumption that all cells are alive at each time point (overall population specific growth rate). Open symbols represent the calculated normalized growth rates with the measured viability at each time point (live cells specific growth rate). Data are mean  $\pm$  SD ( $n=2$ ).

of magnitude higher than the concentrations of mercury found in natural waters. Levels of total Hg in filtered coastal and estuarine environments typically range from 1 to 10 pM, in which MeHg only contributes a small part (<10%) (Fitzgerald et al., 2007).

#### 4.1. Mercury effects on cell morphology

The change in cell size or morphology when the algae were exposed to metals was a common observed toxic effect. Thomas et al. (1980) studied the morphological aberrations of several algae under stress caused by eleven metals, and reported that granular cytoplasm, injured chloroplast integrity, abnormal chains and frustules occurred in time sequence. Similar to their results, SSC signals (indicating the internal complexity or granularity of cells) were more sensitive than FSC signals (indicating the size of cells). In this study, significant increase in cell complexity appeared after 14 h of exposure at the concentrations of 0.2  $\mu$ M for Hg(II) and 9.3 nM for MeHg, respectively, while obviously variation in cell size happened after longer incubation time or at higher exposure concentration. For Hg(II), increased cell complexity may result from chloroplast dispersion, increased grana stacks, dilation of the endoplasmic reticulum and swelling of mitochondrial tubuli (Heumann, 1987). In addition, the FCM side scatter signals were also largely influenced by cell size. The increase in cell size was partly due to the formation of abnormal chains, e.g., daughter cells (2–4 cells) were weakly attached to each other without chitinous connecting threads (Thomas et al., 1980). In addition, metal-induced change in membrane permeability, followed by increased vacuole volume (Linda, 1982), was also part of the cause. Compared with Hg(II), similar but more apparent phenomenon took place for MeHg, even though the basic mechanisms were still not clear.

#### 4.2. Mercury effects on photosynthesis

Autofluorescence intensity had linear relationship with chlorophyll *a* content in *T. weissflogii* cells (Sosik et al., 1989). Our results showed that autofluorescence signals decreased significantly at higher exposure concentration both for Hg(II) and MeHg, with a few exceptions noted. Such trend may be caused by the inhibition effects of Hg(II)/MeHg on the chlorophyll biosynthesis in algal cells (Matson et al., 1972). Besides, the decline in absorption efficiency of chlorophyll *a* under Hg(II) exposure (Slovacek and Hannan, 1977) also contributed to the fluorescence reduction.

In addition, Hg(II) could strongly inhibit photosynthetic electron transport reactions in algae and higher plants (Krupa and Baszyński, 1995). By using the two-photon excitation fluorescence lifetime imaging, we found that the response of algae under Hg(II) exposure was comparable to that under [Cd<sup>2+</sup>] exposure (Zeng et al., unpublished data), indicating an injury to the photosystem. The reason for longer fluorescence lifetime is the toxic effect of Hg(II) on photosynthetic electron transport chain, e.g., Hg(II) could decrease the capacity of photosystem to dissipate the excitation light energy via the photochemical pathway. Previous results showed that Hg(II) was involved in the destruction of oxygen evolving complex (OEC) polypeptide composition (Bernier and Carpentier, 1995), interacting with the cofactors in OEC (Bernier et al., 1993), substituting Cu on plastocyanin (Rai et al., 1991), disturbing the F<sub>B</sub> iron–sulfur cluster (Jung et al., 1995), and interfering with light harvesting complex II (Nahar and Tajmir-Riahi, 1995). The increased fluorescence lifetime was consistent with that measured by pulse-amplitude-modulation fluorescence method when algae were exposed to Hg(II) (Juneau et al., 2001). However, the fluorescence lifetime showed significant increase even when the growth inhibition was negligible, indicating that it had the potential to serve as a more sensitive biomarker.

Quite different from Hg(II), MeHg could not affect the fluorescence lifetime distribution at all, even though the concentration was high enough to cease the cell growth. MeHg showed inhibition effects on photosynthesis in both higher plants and algae (Lipse, 1970; Antal et al., 2009; Matorin et al., 2009). The no obvious effect found in our study may be due to the higher exposure concentrations (10<sup>-7</sup> to 10<sup>-6</sup> M) or different tested organisms used in previous studies. According to our results, MeHg exhibited no toxic effects on the electron transport chain in *T. weissflogii*, suggesting that the intracellular target site of MeHg was not located on the photosynthetic electron transport chain.

#### 4.3. Mercury effects on population growth

MeHg was much more toxic than Hg(II) to the growth of algae, and such variations were partly due to their differences in toxic patterns. The inhibition effect of Hg(II) was to decrease the cell viability or the numbers of cells that continued to divide normally. This was in line with the calculated specific growth rate of live cells, which was not different from that of the control ones (except for the 0.9  $\mu$ M treatment). We proposed that the growth inhibition upon Hg(II) exposure was a combination of subpopulations that reproduced with normal generation time and that could not divide at all. MeHg exposure caused different behavior. MeHg hardly killed the cells (viability higher than 80%), even when the population growth was completely arrested. At each MeHg concentration, the specific growth rates of live cells and total cells were comparable, indicating that the growth inhibition under MeHg stress mainly resulted from an overall slower growth rate of all cells. Even though the toxic mechanisms of Hg(II) and MeHg in algal cells were not investigated here, several previous findings may be closely related to their differences. Firstly, the way of metal is taken up by algae may be different between Hg(II) and MeHg. The accumulation of Hg(II) into cells is passive transport (Fisher and Wente, 1993), while for MeHg the controversies of the way of uptake still continue. Mason et al. (1996) suggested that passive uptake dominated the accumulation of MeHg, whereas Moye et al. (2002) and Pickhardt and Fisher (2007) demonstrated that the uptake of MeHg involved active transport mechanisms. Secondly, differences were also found between the subcellular distributions of Hg and MeHg (Wu and Wang, 2011). For example, the cellular debris (containing cell wall, membranes) was an important binding site for Hg(II), while the heat-stable proteins were a major binding pool for MeHg. This evidence indicated that the intracellular targets of Hg(II) and MeHg as well as the resistance mechanisms of algae to Hg(II) and MeHg were different. Besides, distinguishing the cells that divided normally with those divided slowly may help to understand the recovery process after Hg(II) and MeHg exposure.

#### 4.4. Dark/light cycle

In most species of phytoplankton, cell division was mainly restricted to the dark period (Nelson and Brand, 1979; Rioboo et al., 2009). As an exception, the division of diatom continued throughout the 24 h photocycles (Chisholm and Costello, 1980). This was also demonstrated in the present study that *T. weissflogii* showed continual division during both the light and dark periods, and there was no significant difference for the specific growth rate between these two periods. Such exceptional division patterns may explain the different diel patterns of cell size between *T. weissflogii* (decreased during daytime and increased at night) under lower Hg(II)/MeHg exposure and other phytoplankton species (increased during daytime and decreased at night) (Jacquet et al., 2001).

## 5. Conclusion

Our study demonstrated that the toxic mechanisms of Hg(II) and MeHg in algal cells were quite different. For photosynthesis, Hg(II) increased the average lifetime of chlorophyll fluorescence by blocking the electron transport chain. However, MeHg had hardly affected this sensitive parameter, indicating different intracellular targets compared with Hg(II). For population development, FCM data showed that the growth inhibition caused by Hg(II) was mainly due to the increased injured cells, whereas live cells kept at normal reproduce rate. In contrast, the decreased growth rate under MeHg stress was mainly attributed to the reduced division rate of all cells. In addition, as observed visually and quantitatively by these two noninvasive methods (FLIM and FCM), there were significant morphological changes of diatom cells under Hg(II)/MeHg exposure, which were closely related to the intracellular damage and abnormal division.

## Acknowledgments

We thank the two anonymous reviewers for their comments. This study was supported by the CAS (Chinese Academy of Sciences)/SAFEA (State Administration of Foreign Experts Affairs) International Partnership Program for Creative Research Teams (KZCX2-YW-T001) and a General Research Fund from the Hong Kong Research Grants Council (663009) to W.-X.W.

## References

- Antal, T.K., Graevskaya, E.E., Matorin, D.N., Volgusheva, A.A., Osipov, V.A., Krendeleva, T.E., Rubin, A.B., 2009. Assessment of the effects of methylmercury and copper ions on primary processes of photosynthesis in green microalga *Chlamydomonas moewusii* by analysis of the kinetic curves of variable chlorophyll fluorescence. *Biophysics* 54, 481–485.
- Bernier, M., Carpentier, R., 1995. The action of mercury on the binding of the extrinsic polypeptides associated with the water oxidizing complex of photosystem II. *FEBS Lett.* 360, 251–254.
- Bernier, M., Popovic, R., Carpentier, R., 1993. Mercury inhibition at the donor side of photosystem II is reversed by chloride. *FEBS Lett.* 321, 19–23.
- Broess, K., Borst, J.W., Van Amerongen, H., 2009. Applying two-photon excitation fluorescence lifetime imaging microscopy to study photosynthesis in plant leaves. *Photosynth. Res.* 100, 89–96.
- Chisholm, S.W., Costello, J.C., 1980. Influence of environmental factors and population composition on the timing of cell division in *Thalassiosira fluviatilis* (Bacillariophyceae) grown on light/dark cycles. *J. Phycol.* 16, 375–383.
- Clarkson, T.W., 1997. The toxicology of mercury. *Crit. Rev. Clin. Lab. Sci.* 34, 369–403.
- Czechowska, K., Van Der Meer, J.R., 2011. A flow cytometry based oligotrophic pollutant exposure test to detect bacterial growth inhibition and cell injury. *Environ. Sci. Technol.* 45, 5820–5827.
- Eisler, R., 1987. Mercury hazards to fish, wildlife, and invertebrates: a synoptic review. *Biology Report* 85 (1.10). U.S. Fish and Wildlife Services, Washington, DC.
- Fisher, N.S., Wente, M., 1993. The release of trace elements by dying marine phytoplankton. *Deep Sea Res. P.* 40, 671–694.
- Fitzgerald, W.F., Lamborg, C.H., Hammerschmidt, C.R., 2007. Marine biogeochemical cycling of mercury. *Chem. Rev.* 107, 641–662.
- Franklin, N.M., Adams, M.S., Stauber, J.L., Lim, R.P., 2001. Development of an improved rapid enzyme inhibition bioassay with marine and freshwater microalgae using flow cytometry. *Arch. Environ. Contam. Toxicol.* 40, 469–480.
- Heumann, H.G., 1987. Effects of heavy metals on growth and ultrastructure of *Chara vulgaris*. *Protoplasma* 136, 37–48.
- Iwai, M., Yokono, M., Inada, N., Minagawa, J., 2010. Live-cell imaging of photosystem II antenna dissociation during state transitions. *Proc. Natl. Acad. Sci. U.S.A.* 107, 2337–2342.
- Jacquet, S., Partensky, F., Lennon, J.-F., Vaulot, D., 2001. Diel patterns of growth and division in marine picoplankton in culture. *J. Phycol.* 37, 357–369.
- Juneau, P., Dewez, D., Matsui, S., Kim, S.-G., Popovic, R., 2001. Evaluation of different algal species sensitivity to mercury and metolachlor by PAM-fluorometry. *Chemosphere* 45, 589–598.
- Jung, Y.-S., Yu, L., Golbeck, J.H., 1995. Reconstitution of iron-sulfur center  $F_B$  results in complete restoration of NADP<sup>+</sup> photoreduction in Hg-treated photosystem I complexes from *Synechococcus* sp. PCC 6301. *Photosynth. Res.* 46, 249–255.
- Krupa, Z., Baszyński, T., 1995. Some aspects of heavy metals toxicity towards photosynthetic apparatus – direct and indirect effects on light and dark reactions. *Acta Physiol. Plant.* 17, 177–190.
- Linda, S.G., 1982. A morphometric analysis of algal response to low dose, short-term heavy metal exposure. *Protoplasma* 110, 75–86.
- Lipse, R.L., 1970. Accumulation and physiological effects of methyl mercury hydroxide on maize seedlings. *Environ. Pollut.* 8, 149–155.
- Marie, D., Simon, N., Vaulot, D., 2005. Phytoplankton cell counting by flow cytometry. *Algal Culturing Tech.* 25, 3–267.
- Mason, R.P., Reinfelder, J.R., Morel, F.M.M., 1996. Uptake, toxicity, and trophic transfer of mercury in a coastal diatom. *Environ. Sci. Technol.* 30, 1835–1845.
- Matorin, D.N., Osipov, V.S., Seifullina, N.Kh., Venediktov, P.S., Rubin, A.B., 2009. Increased toxic effect of methylmercury on *Chlorella vulgaris* under high light and cold stress conditions. *Microbiology* 78, 321–327.
- Matson, R.S., Mustoe, G.E., Chang, S.B., 1972. Mercury inhibition on lipid biosynthesis in freshwater algae. *Environ. Sci. Technol.* 6, 158–160.
- Mi, H.L., Klughammer, C., Schreiber, U., 2000. Light-induced dynamic changes of NADPH fluorescence in *Synechocystis* PCC 6803 and its *ndhB*-defective mutant M55. *Plant Cell Physiol.* 41, 1129–1135.
- Miao, A.J., Wang, W.-X., Juneau, P., 2005. Comparison of Cd, Cu, and Zn toxic effects on four marine phytoplankton by pulse-amplitude-modulated fluorometry. *Environ. Toxicol. Chem.* 24, 2603–2611.
- Miles, D., Bolen, P., Farag, S., Goodin, R., Lutz, J., Moustafa, A., Rodriguez, B., Weil, C., 1973. Hg<sup>2+</sup> - A DCMU independent electron acceptor of photosystem II. *Biochem. Biophys. Res. Commun.* 50, 1113–1119.
- Moye, H.A., Miles, C.J., Philips, E.J., Sargent, B., Merritt, K.K., 2002. Kinetics and uptake mechanisms for monomethylmercury between freshwater algae and water. *Environ. Sci. Technol.* 36, 3550–3555.
- Murthy, S.D.S., Mohanty, N., Mohanty, P., 1995. Prolonged incubation with low concentration of mercury alters energy transfer and chlorophyll (Chl) *a* protein complexes in *Synechococcus* 6301: changes in Chl *a* absorption and emission characteristics and loss of the F695 emission band. *Biometals* 8, 237–242.
- Nahar, S., Tajmir-Riahi, H.A., 1995. Do metal ions the protein secondary structure of light-harvesting complex of thylakoid membranes. *J. Inorg. Biochem.* 58, 223–234.
- Nelson, D.M., Brand, L.E., 1979. Cell division periodicity in 13 species of marine phytoplankton on a light/dark cycle. *J. Phycol.* 15, 67–75.
- Pickhardt, P.C., Fisher, N.S., 2007. Accumulation of inorganic and methylmercury by freshwater phytoplankton in two contrasting water bodies. *Environ. Sci. Technol.* 41, 125–131.
- Petrásek, Z., Schmitt, F.-J., Theiss, C., Huyer, J., Chen, M., Larkum, A., Eichler, H.J., Kemnitz, K., Eckert, H.-J., 2005. Excitation energy transfer from phycobiliprotein to chlorophyll *d* in intact cells of *Acartyochloris marina* studied by time- and wavelength resolved fluorescence spectroscopy. *Photochem. Photobiol. Sci.* 4, 1016–1022.
- Prokowsky, Z., 1993. Effects of HgCl<sub>2</sub> on long-lived delayed luminescence in *Scenedesmus quadricauda*. *Photosynthetica* 28, 563–566.
- Rai, L.C., Singh, A.K., Mallick, N., 1991. Studies on photosynthesis, the associated electron transport system and some physiological variables of *Chlorella vulgaris* under heavy metal stress. *J. Plant Physiol.* 137, 419–424.
- Rioboo, C., O'Connor, J.E., Prado, R., Herrero, C., Cid, Á., 2009. Cell proliferation alterations in *Chlorella* cells under stress conditions. *Aquat. Toxicol.* 94, 229–237.
- Šeršeň, F., Král'ová, K., Bumbálová, A., 1998. Action of mercury on the photosynthetic apparatus of spinach chloroplasts. *Photosynthetica* 35, 551–559.
- Shapiro, H.M., 1995. *Practical Flow Cytometry*, 3rd ed. Wiley-Liss Inc., New York, 542 pp.
- Singh, D.P., Khare, P., Bisen, P.S., 1989. Effect of Ni<sup>2+</sup>, Hg<sup>2+</sup> and Cu<sup>2+</sup> on growth, oxygen evolution and photosynthetic electron transport in *Cylindrospermum* IU 942. *J. Plant Physiol.* 134, 406–412.
- Slovacek, R.E., Hannan, P.J., 1977. In vivo fluorescence determinations of phytoplankton chlorophyll *a*. *Limnol. Oceanogr.* 22, 919–925.
- Sosik, H.M., Chisholm, S.W., Olson, R.J., 1989. Chlorophyll fluorescence from single cells: interpretation of flow cytometric signals. *Limnol. Oceanogr.* 34, 1749–1761.
- Thomas, W.H., Hollibaugh, J.T., Seibert, D.L.R., 1980. Effects of heavy metals on the morphology of some marine phytoplankton. *Phycologia* 19, 202–209.
- Tirlapur, U.K., König, K., 2001. Femtosecond near-infrared lasers as a novel tool for non-invasive real-time high-resolution time-lapse imaging of chloroplast division in living bundle sheath cells of *Arabidopsis*. *Planta* 214, 1–10.
- Wang, M.J., Wang, W.-X., 2008. Cadmium toxicity in a marine diatom as predicted by the cellular metal sensitive fraction. *Environ. Sci. Technol.* 42, 940–946.
- Wang, Y.Y., Hammes, F., Roy, K.D., Verstraete, W., Boon, N., 2010. Past, present and future applications of flow cytometry in aquatic microbiology. *Trends Biotechnol.* 28, 416–424.
- Wu, Y., Wang, W.-X., 2011. Accumulation, subcellular distribution and toxicity of inorganic mercury and methylmercury in marine phytoplankton. *Environ. Pollut.* 159, 3097–3105.